

2010-05-01

Highly Visible Light Active TiO₂-xNx Heterojunction Photocatalysts

Vinodkumar Etacheri
Technological University Dublin

Michael Seery
Technological University Dublin, michael.seery@tudublin.ie

Steven Hinder
University of Surrey

See next page for additional authors

Follow this and additional works at: <https://arrow.tudublin.ie/cenresart>

 Part of the [Chemistry Commons](#)

Recommended Citation

Etacheri, V., Seery, M., Hinder, S., Pillai, S. (2010) : Highly Visible Light Active TiO₂-xNx Heterojunction Photocatalysts. *Chemistry of Materials*, Vol. 22, 2010, pp.3843–3853. doi:10.1021/cm903260f

This Article is brought to you for free and open access by the Crest: Centre for Research in Engineering Surface Technology at ARROW@TU Dublin. It has been accepted for inclusion in Articles by an authorized administrator of ARROW@TU Dublin. For more information, please contact arrow.admin@tudublin.ie, aisling.coyne@tudublin.ie, vera.kilshaw@tudublin.ie.

Authors

Vinodkumar Etacheri, Michael Seery, Steven Hinder, and Suresh Pillai

Antenna & High Frequency Research Centre

Articles

Dublin Institute of Technology

Year 2010

Highly Visible Light Active TiO₂-xN_x
Heterojunction Photocatalysts

Suresh C. Pillai
DIT, suresh.pillai@dit.ie

Michael K. Seery
DIT, michael.seery@dit.ie

— Use Licence —

Attribution-NonCommercial-ShareAlike 1.0

You are free:

- to copy, distribute, display, and perform the work
- to make derivative works

Under the following conditions:

- Attribution.
You must give the original author credit.
- Non-Commercial.
You may not use this work for commercial purposes.
- Share Alike.
If you alter, transform, or build upon this work, you may distribute the resulting work only under a license identical to this one.

For any reuse or distribution, you must make clear to others the license terms of this work. Any of these conditions can be waived if you get permission from the author.

Your fair use and other rights are in no way affected by the above.

This work is licensed under the Creative Commons Attribution-NonCommercial-ShareAlike License. To view a copy of this license, visit:

- URL (human-readable summary):
<http://creativecommons.org/licenses/by-nc-sa/1.0/>
 - URL (legal code):
<http://creativecommons.org/worldwide/uk/translated-license>
-

Highly Visible Light Active TiO_2-xN_x Heterojunction Photocatalysts[†]Vinodkumar Etacheri,^{‡,§} Michael K. Seery,[§] Steven J. Hinder,^{||} and Suresh C. Pillai^{*,‡}[‡]Centre for Research in Engineering Surface Technology (CREST), FOCAS Institute, and
[§]School of Chemical and Pharmaceutical Sciences, Dublin Institute of Technology, Kevin Street, Dublin 8,
Ireland, and ^{||}The Surface Analysis Laboratory, Faculty of Engineering and Physical Sciences,
University of Surrey, Guildford, Surrey, GU2 7XH, United Kingdom

Received October 23, 2009. Revised Manuscript Received May 10, 2010

Nitrogen doped anatase-rutile heterojunctions are successfully synthesized through an ethylenediaminetetraacetic acid (EDTA) modified sol–gel process. An FT-IR study of EDTA modified TiO_2 gel confirms the existence of an ionic intermediate (as indicated by a $\Delta\nu$ value of 233 cm^{-1}). Differential scanning calorimetry (DSC), X-ray diffraction (XRD), and Raman spectroscopy are employed to study the phase evolution, phase purity, and crystallite size of samples. Formations of O–Ti–N and N–Ti–N bonds in calcined samples are confirmed using XPS and FT-IR spectroscopy. All EDTA modified samples show significantly higher visible light photocatalytic activity than the unmodified sample. The most active nitrogen doped heterojunction obtained at $400\text{ }^\circ\text{C}$ exhibits 9-fold visible light activity in comparison to the standard photocatalyst Degussa P-25. It is proposed that the photo excited electrons (from the visible midgap level) are effectively transferred from the conduction band of anatase to that of rutile causing effective electron–hole separation, which is responsible for the higher visible light activity and lower photoluminescence (PL) intensity.

1. Introduction

Unique properties of nanosized catalysts such as quantum confinement and high surface to volume ratio make them highly efficient. Among various catalysts, titania nanomaterials find wide applications in the field of solar cells,¹ organic synthesis,² water and air purification,³ cancer therapy,⁴ cathodic corrosion protection, and self-cleaning antibacterial materials.^{5,6} High redox potential, chemical stability, inexpensiveness, and non toxicity of titania made it superior to other semiconductor photocatalysts in its class. Among the three polymorphs, it is generally agreed that the anatase phase has the highest photoactivity followed by rutile and brookite. The efficiency of titania photocatalysts strongly depends on several factors, including phase purity, surface area, crystallite size, amount and nature of dopants, method of preparation, and anatase-rutile ratio.^{7–9}

The wide band gap (3.2 eV) of the anatase titania confines its application to UV light ($\lambda \leq 387.5\text{ nm}$) activation. Even though the high temperature stable rutile phase can absorb visible light (up to $\sim 412\text{ nm}$), its activity is limited as a result of low surface area, low redox potential, and faster electron hole recombination rate.¹⁰ The development of a highly visible light active catalyst is necessary to effectively exploit sunlight or light from artificial sources. Various methods such as metal or non-metal doping, using reduced forms of TiO_x ($X < 2$) photocatalyst, dye sensitization, and optimization of phase composition has been investigated by previous researchers.^{11–13}

Titania doped with main group elements has attracted great interest after the report of nitrogen and other anion (S, C, and F) doped visible-light active (VLA) titania catalyst by Asahi and co-workers.¹⁴ These second-generation TiO_2 materials were photoactive over the UV and visible-light region. Controversy still remains about the nature of the dopant species and electronic structure of nitrogen doped titania, which is highly dependent on the method of preparation. Some researchers proposed the existence of surface adsorbed NO_x and NH_x , while others proposed the presence of lattice nitrogen. Recently, Valentine et al. demonstrated the electronic structure of nitrogen doped

[†] This paper is dedicated to Professor John M. Kelly, C. Chem. FRSC on the occasion of completing his 37 years of teaching and research (celebration of chemistry) at the Trinity College Dublin, Ireland.

*To whom correspondence should be addressed. E-mail: suresh.pillai@dit.ie.

- (1) O'Regan, B.; Grätzel, M. *Nature* **1991**, *353*, 737.
- (2) Kraeutler, B.; Bard, A. J. *J. Am. Chem. Soc.* **1978**, *100*, 2239.
- (3) Ollis, D. F.; Al-Ekabi, H. *Photocatalytic Purification and Treatment of Water and Air*; Elsevier: Amsterdam, The Netherlands, 1993.
- (4) Cai, R.; Kubota, Y.; Shuin, T.; Sakai, H.; Hashimoto, K.; Fujishima, A. *Cancer Res.* **1992**, *52*, 2346.
- (5) Yuan, J.; Tsujikawa, S. *J. Electrochem. Soc.* **1995**, *142*, 3444.
- (6) Honda, H.; Ishizaki, A.; Soma, R.; Hashimoto, K.; Fujishima, A. *J. Illum. Eng. Soc.* **1998**, *42*.
- (7) Kavan, L.; Grätzel, M.; Gilbert, S. E.; Klemenz, C.; Scheel, H. J. *J. Am. Chem. Soc.* **1996**, *118*, 6716–6723.
- (8) Toyoda, M.; Nanbu, Y.; Nakazawa, Y.; Hirano, M.; Inagaki, M. *Appl. Catal., B* **2004**, *49*, 227.
- (9) Beyers, E.; Cool, P.; Vansant, E. F. *J. Phys. Chem. B* **2005**, *109*, 10081.

- (10) Miyagi, T.; Kamei, M.; Mitsuhashi, T.; Ishigaki, T.; Yamazaki, A. *Chem. Phys. Lett.* **2004**, *390*, 399–402.
- (11) Kang, M. G.; Park, N. G.; Park, Y. J.; Ryu, K. S.; Chang, S. H. *Sol. Energy Mater. Sol. Cells* **2003**, *75*, 475.
- (12) Semon, U.; Bahnmann, D.; Testa, J. J.; Rodríguez, D.; Litter, M. I.; Bruno, N. *J. Photochem. Photobiol., A* **2002**, *148*, 247.
- (13) Nakamura, I.; Negishi, N.; Kutsuna, S.; Ihara, T.; Sugihara, S.; Takeuchi, K. *J. Mol. Catal. A: qChem.* **2000**, *161*, 205.
- (14) Asahi, R.; Morikawa, T.; Ohwaki, T.; Aoki, K.; Taga, Y. *Science* **2001**, *293*, 269–275.

titania synthesized through various routes.¹⁵ Density functional theory (DFT) calculations show that substitutional nitrogen atoms create an energy level just above the valence band, where as interstitial nitrogen energy levels lie higher in the gap. Calculations also showed that nitrogen doping leads to an ample lowering of oxygen vacancy formation energy. Photoelectrochemical studies of nitrogen doped titania revealed the formation of additional energy states positioned energetically 1.3 eV broad range just below the conduction band edge. These energy levels cause higher loss of visible light excited charge carriers as a result of recombination.¹⁶ Increasing the doping density also enhances the electron–hole recombination as a result of the reduced band gap. These main drawbacks of nitrogen doped titania limit its visible light activity and applications. For efficient visible light photocatalysis, coupling of nitrogen doped titania with the electron hole separating agents are necessary.

One way to attain high activity is proper designing of heterojunctions with smaller band gap semiconductors, such as rutile. A mixture of anatase and rutile can often outperform the photoactivity of pure anatase or rutile. Recent studies explained the visible light induced production of charges in smaller band gap rutile phase and its transfer to the trapping states of anatase phase.¹⁷ Since the conduction band level of rutile is below that of anatase, photo generated electrons from the conduction band of anatase can be effectively transferred to that of rutile leading to slow electron hole recombination.^{7,18} These two key factors are reported to be responsible for the superior photocatalytic activity of Degussa P25, which has an anatase-rutile ratio of 70/30.¹⁹ Most of the synthesis methods of titania gives anatase rutile mixtures only above 600 °C resulting in a deviation from nanoregime and a subsequent decrease in photocatalytic activity. Nitrogen doping also results in the formation of high temperature stable anatase phase titania.^{20–22} Under these circumstances, it is necessary to develop a low temperature method for the synthesis of nitrogen doped anatase-rutile nano heterojunctions. This has been achieved through an ethylenediaminetetraacetic acid (EDTA) modified sol–gel process, which proceeds through an ionic intermediate [Ti (H₂O) (edta)]. This method proceeds through a solution phase without the formation of polymeric chains, which can ensure better homogeneity and effective doping than conventional sol–gel processes. Both low temperature

crystallizations of anatase-rutile heterojunctions and nitrogen doping were achieved using EDTA. Nishide et al. studied the crystal structure and optical properties of TiO₂ materials prepared from Ti-EDTA complexes.²³ High photocatalytic activities of anatase-brookite and anatase-carbon nanotubes heterojunctions have also been reported.^{24,25} However, to the best of our knowledge, there is no systematic study available on a highly visible light active TiO_{2-x}N_x anatase-rutile heterojunction photocatalysts. The current study focuses on the low temperature crystallization, mechanism of formation, and the photocatalytic activity of TiO_{2-x}N_x heterojunctions.

2. Experimental Methods

2.1. Synthesis of N-Doped Titania Heterojunctions. All reagents were used without further purification. Titanium isopropoxide (Aldrich 97%) and EDTA (Aldrich 99.99%) was used as the titania precursor and modifier respectively. In a typical synthesis for 1:1 EDTA modified sample, titanium isopropoxide (9 mL) was dissolved in isopropanol (23 mL). This solution was mixed with glacial acetic acid (1.7 mL) and EDTA (8.8 g). The precipitate obtained was then mixed with deionized water (55 mL) and stirred for 2 h to form a sol. The sol obtained was then heated in an oven at 80 °C to form a solution, which on further heating converts to a gel. Xerogel thus obtained after 24 h was calcined at 400, 500, 600, 700, 800, and 900 °C for 2 h at a heating rate of 10 °C/min. Various molar ratios of TTIP/IPA/ACOH/H₂O/EDTA were used for the synthesis of different samples (Supporting Information 15). All nitrogen doped heterojunctions were prepared by successively replacing 0.5 molar ratios of acetic acid by EDTA (identified as 0.5 ED-TiO₂, 1.0 ED-TiO₂, 1.5 ED-TiO₂, and 2.0 ED-TiO₂ respectively after calcination). Ratios between other reagents were maintained as constant in all synthesis. The control sample without EDTA was also prepared using the same synthesis method. Molar ratio between titanium isopropoxide, acetic acid, isopropanol, and water was 1:2:10:100 for the synthesis of the control sample. Degussa P-25 was used as the standard TiO₂ sample for comparison.

2.2. Characterization Techniques. The FTIR spectra of xerogel dried at 100 °C and calcined at different temperatures were recorded using a Perkin-Elmer GX-FTIR spectrometer in the range 4000–400 cm⁻¹. Transparent pellets were prepared using a 4 mm dye after mixing samples with KBr. Rheometric Scientific DSC QC and Shimadzu DTG-60 instruments were used for differential scanning calorimetry (DSC) and differential thermal analysis (DTA) respectively. In both cases, about 5 mg of dried gel was heated from room temperature (25 °C) to 600 °C at a constant heating rate of 10 °C/min. The crystal phases of calcined samples were analyzed by X-ray diffraction using a Siemens D500 X-ray diffractometer (2θ = 10–70°) working with Cu–Kα radiation (λ = 0.15418 nm). The Spurr equation (eq 1) was employed for the precise calculation of the amount of rutile in the sample.

$$F_R = \frac{1}{1 + 0.8[I_A(101)/I_R(110)]} \quad (1)$$

- (15) Valentin, C. D.; Pacchioni, G.; Selloni, A.; Livraghi, S.; Giamello, E. *J. Phys. Chem. B* **2005**, *109*, 11414–11419.
 (16) Torres, G. R.; Lindgren, T.; Lu, J.; Granqvist, C.-G.; Lindquist, S.-E. *J. Phys. Chem. B* **2004**, *108*, 5995–6003.
 (17) Junin, C.; Thanachayanont, C.; Euvananont, C.; Inpor, K.; Limthongkul, P. *Eur. J. Inorg. Chem.* **2008**, 974–979.
 (18) Kawahara, T.; Konishi, Y.; Tada, H.; Tohge, N.; Nishii, J.; Ito, S. *Angew. Chem., Int. Ed.* **2002**, *41*(15), 2811–2813.
 (19) Balasubramanian, G.; Dionysiou, D. D.; Suidan, M. T.; Baudin, I.; Laine, J. M. *Appl. Catal., B* **2004**, *47*, 73–84.
 (20) Pillai, S. C.; Periyat, P.; George, R.; McCormack, D. E.; Seery, M. K.; Hayden, H.; Colreavy, J.; Corr, D.; Hinder, S. J. *J. Phys. Chem. C* **2007**, *111*, 1605–1611.
 (21) Sato, S.; Nakamura, R.; Abe, S. *Appl. Catal., A* **2005**, *284*, 131.
 (22) Mwabora, J. M.; Lindgren, T.; Avendano, E.; Jaramillo, T. F.; Lu, J.; Lindquist, S. E.; Granqvist, C. G. *J. Phys. Chem. B* **2004**, *108*, 20193.

- (23) Nishide, T.; Sato, M.; Hara, H. *J. Mater. Sci.* **2000**, *35*, 465–469.
 (24) Tian, G.; Fu, H.; Jing, L.; Xin, B.; Pan, K. *J. Phys. Chem. C* **2008**, *112*, 3083–3089.
 (25) Wang, H.; Quan, X.; Yu, H.; Chen, S. *Carbon* **2008**, *46*, 1 1 2 6–1 1 3 2.

159 Where F_R is the mass fraction of rutile, $I_A(101)$ and $I_R(110)$ are
 160 the integrated main peak intensities of anatase and rutile,
 161 respectively. Crystallite sizes of anatase and rutile in calcined
 162 samples were calculated using the Scherrer equation (eq 2).

$$\Phi = \frac{k\lambda}{\beta \cos \theta} \quad (2)$$

163 Where Φ is the crystallite size, k is the shape factor, λ is the X-ray
 164 radiation wavelength, and β the full line width at half-maximum
 165 height of the main intensity peak after subtraction of the equip-
 166 ment line broadening. Raman spectra of all samples were recor-
 167 ded at room temperature with a Dilor ISA Labram 1 B micro-
 168 Raman system equipped with a 514 nm Ar⁺ ion laser (Laser
 169 Physics Reliant 150 Select Multi-Line). Measurements were
 170 carried out on powder samples at a laser power of 3 mW to
 171 avoid excessive heating.

172 X-ray photoelectron spectroscopy (XPS) analyses were per-
 173 formed on a Thermo VG Scientific Sigma Probe spectrometer
 174 using monochromatic Al-K α radiation (photon energy 1486.6
 175 eV). For Ti 2p high-resolution spectra pass energy of 20 eV and a
 176 0.1 eV step size were used. A pass energy of 50 eV and a step size
 177 of 0.2 eV were used for N 1s high-resolution spectra. Charge
 178 compensation was achieved by using a low-energy electron
 179 flood gun. Quantitative surface chemical analyses were calcu-
 180 lated from the high-resolution core level spectra, following the
 181 removal of a nonlinear Shirley background. Absorbance spectra
 182 of the samples were recorded in the diffuse reflectance mode
 183 (with an integrated sphere attachment) using a Perkin-Elmer
 184 Lambda 900 UV/vis/NIR spectrometer, using BaSO₄ as the
 185 reference sample (in the range of 300–600 nm). Sample pellets
 186 were prepared using a 4 mm die after thoroughly mixing the
 187 powder samples with KBr. The band gaps were calculated by
 188 extrapolating the lower wavelength cutoff region. Samples for
 189 photoluminescence studies were prepared by dispersing as pre-
 190 pared powders (0.01 g in 100 mL) in deionized water. All samples
 191 were sonicated for 30 min before analysis. Room temperature
 192 emission spectra of samples were obtained from Perkin-Elmer
 193 Luminescence Spectrometer (LS-55) at an excitation wavelength
 194 of 260 nm in the range 300 to 800 nm.

195 Nitrogen adsorption and desorption isotherms were collected
 196 at liquid nitrogen temperature using a Quantachrome 2000e
 197 surface area analyzer. All samples were degassed at 300 °C for
 198 2 h under vacuum prior to the analysis. The specific surface area
 199 was calculated using the linear portion of the Brunauer–
 200 Emmett–Teller (BET) model ($P/P_0 = 0.05–0.2$). Desorption
 201 branch of the Barret–Joyner–Halenda (BJH) model was em-
 202 ployed for the precise determination of pore diameter and
 203 volumes. For transmission electron microscopy (TEM) anal-
 204 ysis, powder samples were suspended in water and sonicated for
 205 30 min before being dispersed onto Formvar-coated copper
 206 grids. The particle-loaded grids were studied under JEOL JEM-
 207 2100 transmission electron microscope operating at an accel-
 208 erating voltage of 200 kV.

209 **2.3. Photocatalysis Study.** Decomposition of methylene blue
 210 was performed to evaluate the photocatalytic activities of samples.
 211 The catalyst (0.06 g) was dispersed in an aqueous solution of
 212 methylene blue (50 mL 1×10^{-5} M) placed in a glass vessel
 213 (100 mL). The vessel was placed in the dark for 30 min and
 214 irradiated with visible light (0.68 W/m^2) using Q-Sun solar simu-
 215 lator and a primary blue filter (450 nm) (Supporting Informa-
 216 tion 13). The temperature of the suspension was maintained
 217 at 25 °C with the help of an air cooler (thermostat attached)
 218 connected to the solar simulator. Degradation of methylene blue

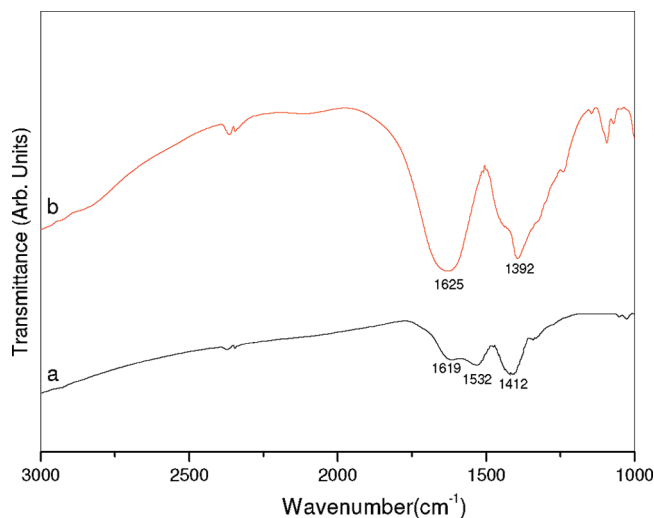


Figure 1. FT-IR Spectrum of 80 °C dried titania precursor (a) acetic acid modified and (b) EDTA modified.

219 was monitored by taking aliquots at equal time intervals of 1 h.
 220 These aliquots were centrifuged, and absorption spectra of the
 221 samples were recorded using Perkin-Elmer Lambda 900 UV/vis/
 222 NIR spectrometer. Similar experiments were carried out for
 223 samples calcined at different temperatures. The rate of degrada-
 224 tion was assumed to obey pseudo-first order kinetics, given
 225 that natural logarithmic plots were linear. The rate constant for
 226 degradation, k , was calculated from the first order plot (eq 3).

$$\ln\left(\frac{A_0}{A}\right) = kt \quad (3)$$

227 Where A_0 is the initial absorbance, A is absorbance after a time
 228 (t), and k is the first order rate constant. All photocatalytic
 229 experiments were triplicated, and the rate constants were within
 230 5% error limit.

3. Results and Discussion

231 **3.1. Characterization of Modified Precursor.** *3.1.1. FT-IR Spectral Studies.* The nature of reaction inter-
 232 mediates formed from acetic acid and EDTA modified
 233 titania precursor was investigated using FT-IR spec-
 234 troscopy. Formation of an ionic Ti-EDTA complex
 235 responsible for the low temperature crystallization of
 236 heterojunctions was observed from this study. The dif-
 237 ference in frequency $\Delta\nu$ between antisymmetric and
 238 symmetric vibrations of C=O bonds are usually related
 239 to the type of coordination (Figure 1) in metal car-
 240 boxylates.²⁶ Acetic acid modified gel exhibits charac-
 241 teristic antisymmetric and symmetric C=O stretching
 242 vibrations at 1532 and 1412 cm⁻¹, respectively.^{27,28} The
 243 $\Delta\nu$ value of 120 cm⁻¹ observed is characteristic of a
 244 bridged acetic acid titanium isopropoxide complex as
 245 reported by Sanchez et al.²⁸ Antisymmetric and sym-
 246 metric C=O stretching vibrations of EDTA modified
 247
 248

(26) Mehrotra, R. C.; Bohra, R. *Metal Carboxylates*; Academic Press: London, 1983; p 48.

(27) Perrin, F. X.; Nguyen, V.; Vernet, J. L. *J. Sol-Gel Sci. Technol.* **2003**, *28*, 205–215.

(28) Doeuff, S.; Henry, M.; Sanchez, C.; Livage, J. *J. Non-Cryst. Solids* **1987**, *89*, 206–216.

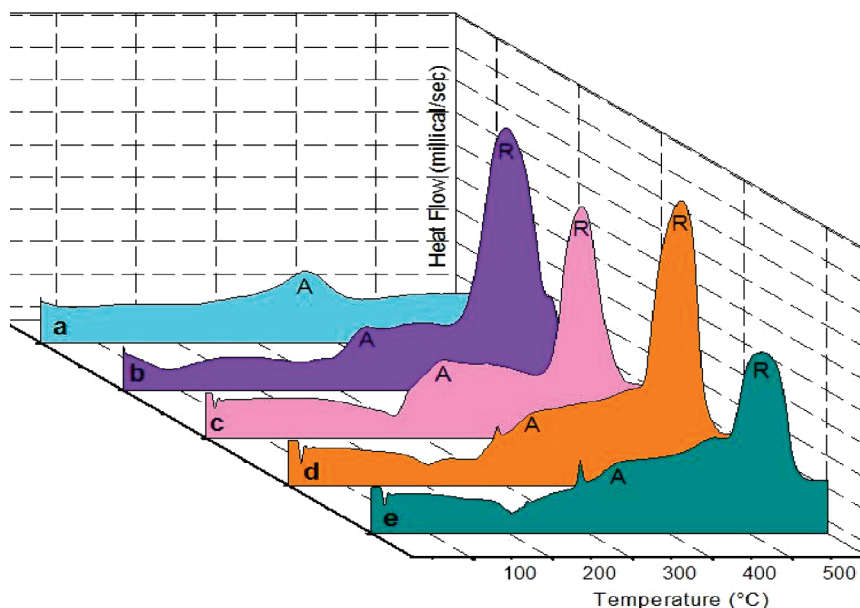


Figure 2. Differential scanning calorimetric pattern of titania gel. (a) Control sample, (b) 0.5 ED-TiO₂, (c) 1.0 ED-TiO₂, (d) 1.5 ED-TiO₂, (e) 2.0 ED-TiO₂.

gel were found at 1625 and 1392 cm⁻¹, respectively. The $\Delta\nu$ value of 233 cm⁻¹ observed for the EDTA modified gel confirmed the monodentate and ionic behavior of COO group in the complex.²⁹ The spectrum of this complex was consistent with that of [Ti(H₂O)(edta)] as observed by Sato et al.³⁰

All EDTA modified samples showed identical FT-IR spectra. The formation of the acetic acid bridged complex was not observed in compositions containing both acetic acid and EDTA. These results indicate a preferential formation of the [Ti(H₂O)(edta)] complex from a mixture of acetic acid, EDTA, and titanium tetraisopropoxide, which can be correlated to the stronger ligand character of EDTA. Variations of ionic character among the different EDTA modified compositions were also investigated. An increase of ionic character was observed as a decrease in antisymmetric stretching frequency values of C=O group (Supporting Information 1). A minimum antisymmetric value of 1600 cm⁻¹ observed for 1:1 EDTA complex indicates it is of the highest ionic character, leading to a lowest thermal stability. This was later confirmed by the completion of phase transformation to rutile at 700 °C (From XRD). Bridged acetate groups in the acetic acid complex effectively alter the condensation pathway and promote the formation of linear polymers. This leads to the formation of anatase titania at higher temperatures, whereas EDTA complex exists as monomers resulting in the low temperature crystallization of anatase and rutile. These results thus confirmed the formation of a high temperature stable covalent acetic acid complex and a thermally less stable ionic EDTA complex of Ti⁴⁺ (Supporting Information 2).

3.1.2. Thermal Stability Analysis of Modified Precursor. Both the amorphous to anatase transition and the anatase-rutile transformation (ART) from acetic acid and

EDTA derived complexes of titania were analyzed using differential scanning calorimetry (DSC) and thermogravimetric analysis (TGA) techniques. For both samples, evaporation of water and acetic acid molecules from the gel was observed as an endothermic DSC peak at 50 °C (Figure 2). The acetic acid complex showed only one exothermic peak at 360 °C representing the crystallization of anatase phase. Anatase to rutile transformation was not observed for this complex up to 600 °C. Removal of coordinated water molecules from the EDTA complexes were observed as an endothermic peak at 265 °C. Since there are no such coordinated water molecules in acetic acid complex, a corresponding peak was not observed in these samples. Among the different EDTA complexes, the most ionic (1:1 EDTA) material shows the lowest anatase and rutile crystallization temperatures of 320 and 498 °C respectively. Slight increases in both temperatures were observed for complexes containing excess EDTA (1:1.5 and 1:2). This may be due to the hindering effect of excess EDTA toward anatase phase evolution and its transformation to rutile. An additional exotherm responsible for the decomposition of unreacted EDTA was also observed at 290 °C in complexes containing excess EDTA (1:1.5 and 1:2).³¹ The formation of anatase-rutile heterojunctions were observed only from EDTA modified titania precursor. In contrast, acetic acid modified precursor shows higher thermal stability. It is thus clear that in the case of EDTA modified samples, amorphous to crystalline as well as anatase to rutile transformations happened at lower temperatures.

The total weight loss calculated for the acetic acid modified complex from the TGA curve was 17%. An increased weight loss of 58% and 85% was observed for 1:0.5 and 1:2.0 EDTA modified compositions respectively

(29) Sawyer, D. T.; MCKinnie, M. *Inorg. Chem.* **1960**, *82*, 4191–4196.
 (30) Sato, M.; Hara, H.; Nishide, T.; Sawada, Y. *J. Mater. Chem.* **1996**, *6*(11), 1767–1770.

(31) Guinesi, L. S.; Ribeiro, C. A.; Crespi, M. S.; Santos, A. F.; Capela, M. V. *J. Therm. Anal. Calorim.* **2006**, *85*, 301–307.

283
 284
 285
 286
 287
 288 F2
 289
 290
 291
 292
 293
 294
 295
 296
 297
 298
 299
 300
 301
 302
 303
 304
 305
 306
 307
 308
 309
 310
 311
 312
 313
 314
 315
 316
 317

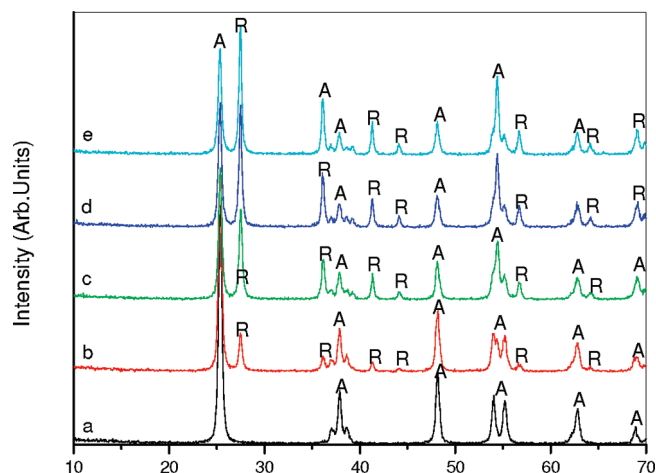


Figure 3. XRD of samples calcined at 600 °C. (a) Control TiO₂, (b) 0.5 ED-TiO₂, (c) 1.0 ED-TiO₂, (d) 1.5 ED-TiO₂, (e) 2.0 ED-TiO₂ (A = anatase; R = rutile).

(Supporting Information 3). The weight losses for the acetic acid complex happen in the range 30–250 °C and 300–500 °C because of the evaporation of solvents and the decomposition of the complex into crystalline anatase titania. On the other hand, the EDTA complex decomposes in three steps (30–150, 250–450, 530–600 °C), a process corresponding to evaporation of solvents, decomposition of EDTA-titania complex into anatase titania, and anatase-rutile transformation, respectively. On increasing the amount of EDTA, a significant increased weight loss in the anatase formation step was observed, which can be due to the decomposition of excess EDTA present in these samples. The lowering of both the anatase and rutile formation temperature was also observed (from the TGA curve) on increasing the amount of EDTA.

3.2. Formation of N-Doped Heterojunctions. 3.2.1.

X-ray Diffraction Studies. X-ray diffraction patterns recorded from samples calcined at different temperatures confirmed the high temperature stability of acetic acid modified samples and low temperature crystallization of N-doped anatase-rutile heterojunctions from EDTA modified samples. The control sample showed only the peaks characteristic of anatase phase up to 600 °C (Figure 3), whereas all EDTA modified samples exist as anatase-rutile mixtures at a temperature as low as 500 °C. The crystallization of anatase-rutile heterojunctions were observed even at 400 °C for 1:1 and 1:1.5 EDTA modified samples (Figure 4). Complete rutile formation for the 1:1 EDTA modified sample (which was found to be the most ionic from FT-IR studies) was observed at 700 °C (Supporting Information 4). Compared to other EDTA modified samples, 1:2.0 modified EDTA sample shows slow anatase rutile transformation kinetics and contains 4% anatase even at 800 °C. All samples calcined at 900 °C exist as 100% rutile (Supporting Information 5). Bridged acetate groups in AcOH-Ti complex effectively alter the condensation pathway and promote the formation of linear polymers. This leads to the formation of anatase titania at higher temperatures, whereas EDTA-Ti complex

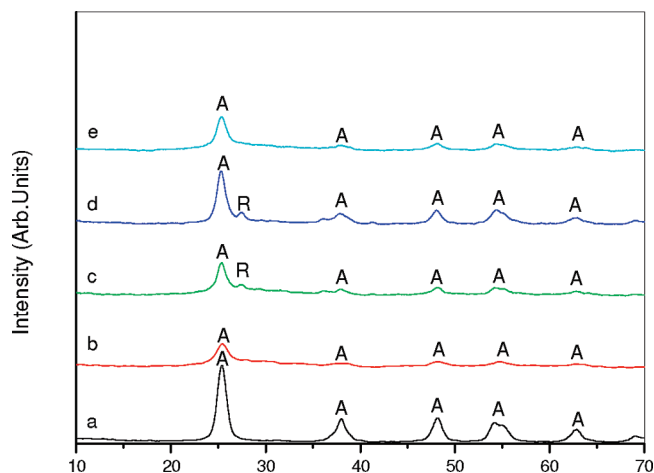


Figure 4. XRD of samples calcined at 400 °C. (a) Control TiO₂, (b) 0.5 ED-TiO₂, (c) 1.0 ED-TiO₂, (d) 1.5 ED-TiO₂, (e) 2.0 ED-TiO₂ (A = anatase; R = rutile).

exists as monomers and results in the low temperature crystallization of both anatase and rutile phases having large crystallite sizes. Slight changes ($2\theta = 0.2^\circ$) in the anatase 110 peak positions for EDTA modified titania samples were observed even at 400 °C compared to the control sample (Supporting Information 6), which results from changes in the lattice parameters as a result of nitrogen doping.³² Thus XRD results revealed the low temperature crystallization of anatase rutile heterojunctions from EDTA modified titania samples and successful lattice incorporation of nitrogen.

3.2.2. Raman Studies. Raman spectroscopy, a more surface sensitive technique was employed as an additional tool to confirm phase composition and surface homogeneity.³³ The Raman active modes for anatase ($A_{1g} + 2B_{1g} + 3E_g$ at 147, 197, 396, 516, and 638 cm^{-1}) and rutile ($A_{1g} + B_{1g} + B_{2g} + E_g$ at 144, 238, 447, and 611 cm^{-1}) were used as fingerprints.^{34–36} The samples 1:1 EDTA and 1:1.5 EDTA calcined at 400 °C has peaks characteristic of anatase rutile mixtures, while other samples show peaks of pure anatase phase (Supporting Information 7). Only the acetic acid modified sample gives peaks of anatase at 600 °C; all EDTA modified samples were anatase-rutile mixtures (Figure 5). All samples calcined at 900 °C shows peaks at 144, 611, 447, and 238 cm^{-1} , which confirmed the existence of 100% rutile phase (Supporting Information 8). Thus the results observed from X-ray diffraction studies were further confirmed by Raman spectroscopy.

3.2.3. FT-IR Spectral Studies. Spectra of heterojunctions obtained were highly dependent on the processing temperature and nature of dopant species (Figure 6). Considerable shifting of Ti–O–Ti stretching frequencies to higher energy was observed for N-doped samples in comparison to the undoped one. At 400 °C, Ti–O–Ti stretching peak of N-doped sample was observed at a

(32) Zhang, Q.; Gao, L. *J. Eur. Ceram. Soc.* **2006**, *26*, 1535–1545.

(33) Gao, K. *Phys. B* **2007**, *398*, 33–37.

(34) Ohsaka, T.; Izumi, F.; Fujiki, Y. *J. Raman Spectrosc.* **1978**, *7*, 321.

(35) Berger, H.; Tang, H.; Lévy, F. *J. Cryst. Growth* **1993**, *130*, 108.

(36) Tang, H.; Prasad, K.; Sanjines, R.; Schmid, P. E.; Levy, F. *J. Appl. Phys.* **1994**, *75*, 2042.

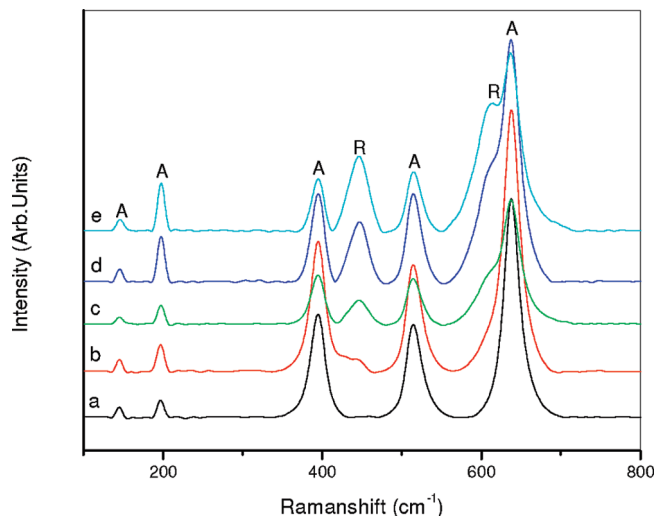


Figure 5. Raman spectra of samples calcined at 600 °C. (a) Control TiO₂, (b) 0.5 ED-TiO₂, (c) 1.0 ED-TiO₂, (d) 1.5 ED-TiO₂, (e) 2.0 ED-TiO₂.

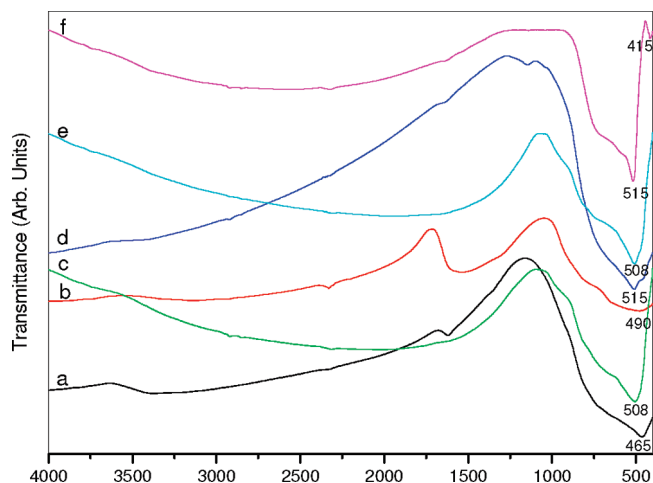


Figure 6. FT-IR Spectrum of calcined titania. (a) Control TiO₂ 400, (b) 0.5 ED-TiO₂ 400, (c) Control TiO₂ 600, (d) 0.5 ED-TiO₂ 600, (e) Control TiO₂ 700, (f) 0.5 ED-TiO₂ 700.

higher energy of 508 cm⁻¹ compared to 465 cm⁻¹ for undoped one. Similar shift in Ti–O–Ti stretching energies were also observed for samples calcined at higher temperatures. These types of shifts to higher energies were previously reported and assigned to the formation of O–Ti–N and N–Ti–N bonds in N-doped titania.³⁷ Since we observed the formation of N–Ti–N bonds as an additional peak at 415 cm⁻¹ in samples calcined at 700 °C,³⁷ shifting observed for Ti–O–Ti stretching energies below this temperature can be assigned to the formation of O–Ti–N bonds through partial replacement of oxygen. No evidence for interstitial nitrogen doping and other nitrogen impurities were observed from the spectra. The lattice incorporation of nitrogen in two different forms was thus observed from FT-IR results. Formations of O–Ti–N and N–Ti–N bonds were also confirmed through XPS studies and will be discussed in the following section.

3.2.4. XPS Studies. XPS results revealed two types of lattice doping (O–Ti–N and N–Ti–N) and a decrease of nitrogen content with an increase of EDTA concentration (Supporting Information 9). An increase of EDTA concentration accelerates crystallite growth (from XRD results), which can decrease the amount N-doping as a result of surface and lattice strain relaxation. Decrease of nitrogen content was also observed with an increase of calcination temperature. This can be due to the crystallite growth and escape of the dopant species formed through the decomposition of Ti-EDTA complex at higher temperatures. The N 1s binding energy peak of N-doped TiO₂ heterojunctions were found to be highly depends on the calcination temperature. In the case of samples calcined at 700 °C, formation of N–Ti–N bonds were observed as a peak at 396 eV (which corresponds to an additional FT-IR peak at 415 cm⁻¹) (Figure 7 b).³⁸ This can be due to the formation of specific Ti–N bonds through an oxygen vacancy compensation mechanism at a higher temperature. Only one peak was observed at 400.1 eV in samples calcined at 600 °C (Figure 7 a), which is a value greater than the typical N 1s binding energy of 397.2 eV in TiN.³⁹ Since FT-IR and XRD results indicate lattice doping, this peak therefore can be attributed to the 1s electron binding energy of the N atom in the environment of O–Ti–N in lattice N-doped titania. The binding energy shifting can be understood by the fact that the N 1s electron binding energy is higher when the formal charge of N is more positive (e.g., 408 eV in NaNO₃), compared to zero or a negative formal charge (398.8 eV in NH₃).^{39,40} When a nitrogen substitutes for the oxygen in the initial O–Ti–O structure, the electron density around N is reduced compared to that in a TiN crystal (because of the O atom on the Ti atom). Thus the N 1s binding energy in an O–Ti–N environment (400.1 eV) is higher than that in an N–Ti–N environment (396 eV) where the N atom replaces the O atom. These observations are consistent with the earlier XPS characterization results associated with the oxidation of TiN surfaces by Saha and Tomkins.³⁹

As reported by Saha and Tomkins, pure titania sample has a typical Ti 2p binding energy of 459.4 eV.³⁹ A decrease of 0.35 and 0.96 eV in Ti 2p binding energy was observed for N-doped heterojunctions obtained at 600 and 700 °C, respectively, in comparison to the standard sample (Figure 8). A decrease of Ti 2p binding energy is a direct measure of the lowering of the valence state level of Ti⁴⁺ to Ti³⁺ and Ti²⁺ level as a result of the lattice substitution of nitrogen for oxygen.^{35,41} Lattice incorporation of nitrogen creates Ti–N bonds by the partial replacement of O²⁻ with N⁻. This results in an electron density decrease and partial reduction of Ti⁴⁺ to Ti³⁺ and Ti²⁺, which reflects as a decrease in Ti 2p binding

(38) Irie, H.; Watanabe, Y.; Hashimoto, K. *J. Phys. Chem. B* **2003**, *107*, 5483.

(39) Saha, N. C.; Tomkins, H. C. *J. Appl. Phys.* **1992**, *72*, 3072.

(40) Chen, X.; Burda, C. *J. Phys. Chem. B* **2004**, *108*, 15446–15449.

(41) Hashimoto, S.; Murata, A.; Sakurada, T.; Tanaka, A. *J. Surf. Anal.* **2002**, *9*, 459.

(37) Jackson, A. W.; Shebanova, O.; Hector, A. L.; McMillan, P. F. *J. Solid State Chem.* **2006**, *179*, 1383–1393.

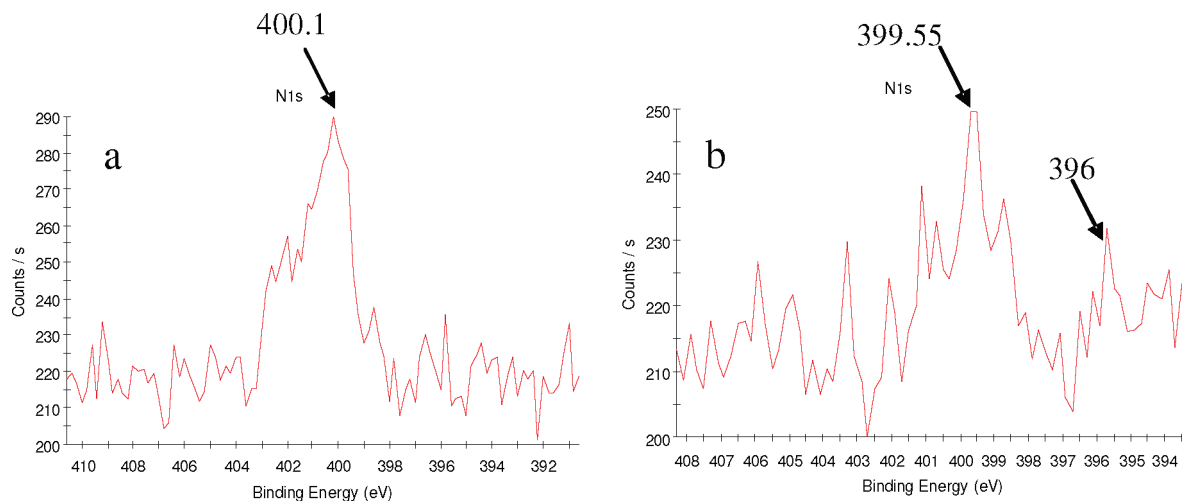


Figure 7. N 1s peaks in the XPS plot of calcined titania. (a) 0.5 ED-TiO₂ 600, (b) 0.5 ED-TiO₂ 700.

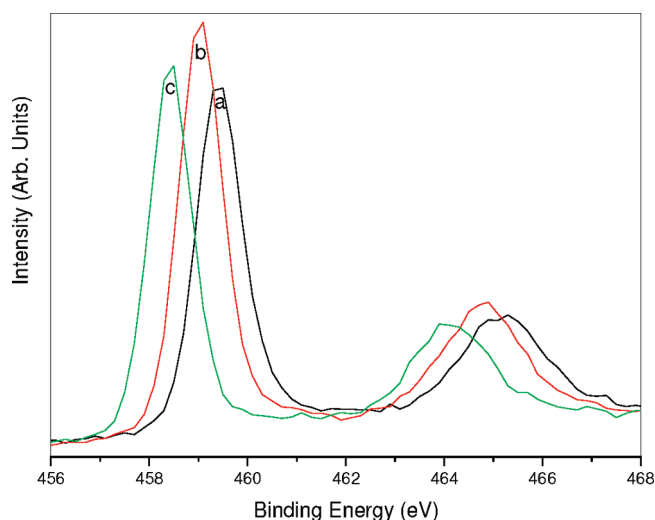


Figure 8. Ti 2p peaks in the XPS plot of calcined titania. (a) Control TiO₂ 600, (b) 0.5 ED-TiO₂ 600, (c) 0.5 ED-TiO₂ 700.

energy.⁴¹ An additional O 1s peak appeared for N-doped heterojunctions at 532 eV (Supporting Information 10), which was first observed by Saha and Tomkins and most recently characterized by Gyorgy et al. in their depth profiling study on TiN surfaces. Gyorgy et al. assigned this feature to the formation of oxidized TiN, which leads to the Ti–O–N structure.⁴² Our study suggests that the appearance of this peak is a consistent feature for the nitrogen substitution in TiO₂ and signifies the formation of O–Ti–N and N–Ti–N structures. Moreover, Rodriguez et al. measured the O 1s peak for -NO and -NO₂ at 533.5 eV,⁴³ compared to the 532 eV value in our study, which can exclude the novel properties related to surface adsorbed nitrogen species. The presence of adventitious elemental carbon was also identified in samples (peak at 285 eV), (Supporting Information 11) which is an

Table 1. Band Gap Values of Heterojunctions Calcined at Different Temperatures

composition	band gap (eV) 400 °C	band gap (eV) 600 °C	band gap (eV) 700 °C
control TiO ₂	3.11	3.16	3.15
0.5 ED-TiO ₂	3.03	3.02	2.98
1.0 ED-TiO ₂	3.00	3.00	2.96
1.5 ED-TiO ₂	2.98	2.98	2.95
2.0 ED-TiO ₂	3.05	2.97	2.93

unavoidable presence on all air-exposed materials.⁴⁴ It is therefore clear from the above observations that the lowering of Ti 2p binding energies and additional O 1s peak observed for N-doped heterojunctions together with FT-IR and XRD results well explained successful lattice incorporation of nitrogen through the formation of O–Ti–N and N–Ti–N bonds.

3.2.5. UV/vis Spectroscopic Studies. Band gap values calculated through diffuse reflectance measurements also support the variations of nitrogen and rutile concentrations in heterojunctions. All N-doped heterojunctions show narrowing of the band gap in comparison to the control sample (Table 1). The narrowing effect was comparatively high for the composition 0.5 ED-TiO₂, which contain the highest amounts of nitrogen at each calcination temperature (Figure 9). Band gap narrowing effect was very low for compositions containing higher amounts of EDTA. This can be due to decreased N-doping as a result of excessive crystallite growth on increasing EDTA concentration. It was previously reported that the nitrogen doping can lead to a mixing of N 2p orbitals with O 2p orbitals to form intermediate energy levels and shift the absorption edge toward visible light region.^{14,45} Nitrogen doping also accelerate the formation of oxygen vacancies, which form additional energy levels below the conduction band. This promotes electronic excitation from the valence band to the additional energy level by absorbing visible light.⁴⁶ A lowering of band gap values through

(42) Gyorgy, E.; Pino, A. P. d.; Serra, P.; Morenza, J. L. *Surf. Coat. Technol.* **2003**, *173*, 265.

(43) Rodriguez, J. A.; Jirsak, T.; Dvorak, J.; Sambasivan, S.; Fischer, D. *J. Phys. Chem. B* **2000**, *104*, 319.

(44) Sakthivel, S.; Kisch, H. *Angew. Chem., Int. Ed.* **2003**, *42*, 4908–4911.

(45) Morikawa, T.; Asahi, R.; Ohwaki, T.; Aoki, K.; Taga, Y. *Jpn. J. Appl. Phys.* **2001**, *40*, L561.

(46) Yang, J.; Bai, H.; Tan, X.; Lian, J. *Appl. Surf. Sci.* **2006**, *253*, 1988–1994.

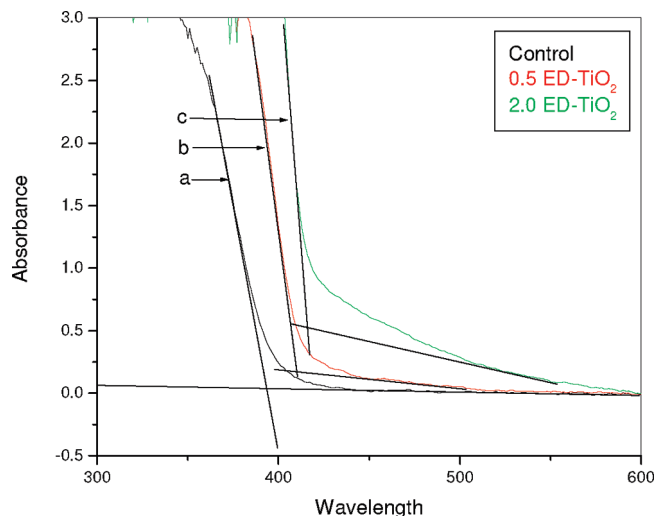


Figure 9. Diffuse reflectance spectra of (a) Control TiO₂ 600, (b) 0.5 ED-TiO₂ 600, and (c) 2.0 ED-TiO₂ 600.

508 both of these mechanisms highly depends on the dopant
509 concentration, which explains the band gap variations
510 observed above.

511 The amount of rutile also plays a significant role to
512 shift the absorption edge of heterojunctions toward the
513 visible light region. Since it is evident from the XPS
514 results that the amount of nitrogen decreases on in-
515 creasing the EDTA content, a decrease in the band gap
516 after the composition 0.5 ED-TiO₂ happens mainly
517 because of rutilation. For this reason, all samples show
518 a decrease in the band gap on increasing the calcination
519 temperature. At 400 °C, band gap narrowing effect was
520 low because of less rutilation at lower temperatures. The
521 superior visible light absorbing capability of hetero-
522 junctions and their dependence on the amount of nitro-
523 gen and rutile were thus verified from diffuse reflectance
524 results.

525 **3.2.6. Surface Area Measurements.** Isotherms of hetero-
526 junctions and the control sample show type IV char-
527 acteristics with H1 type (cylindrical shape) of hysteresis
528 (Figure 10).⁴⁷ The high steepness hysteresis loop ending at
529 a relative pressure (P/P_0) of 0.6 is a measure of high order
530 of mesoporosity in these samples.⁴⁸ Degussa P-25, the
531 standard photocatalyst, has a type II isotherm with
532 small hysteresis behavior (Figure 11). This fact demon-
533 strates the presence of a large quantity of agglomerated
534 particles formed through a diffusion process, which
535 decreases the porosity. Among the different samples
536 compared, the control sample has the highest surface area
537 (134 m²/g) and pore volume (0.209 cc/g) at 400 °C (Table 2).
538 All heterojunction samples have lower surface area com-
539 pared to the control sample at all calcination temperatures.
540 For both heterojunctions and the control sample, a con-
541 siderable decrease in surface area and pore volume was
542 observed with an increase in calcination temperature.

(47) Nasar, R. S.; Cerqueira, M.; Longo, E.; Varela, J. A. *Cerâmica* **2008**, *54*, 38–42.

(48) Kartini, I.; Meredith, P.; Costa, J. C. D. D.; Lu, G. Q. *J. Sol-Gel Sci. Technol.* **2004**, *31*, 185–189.

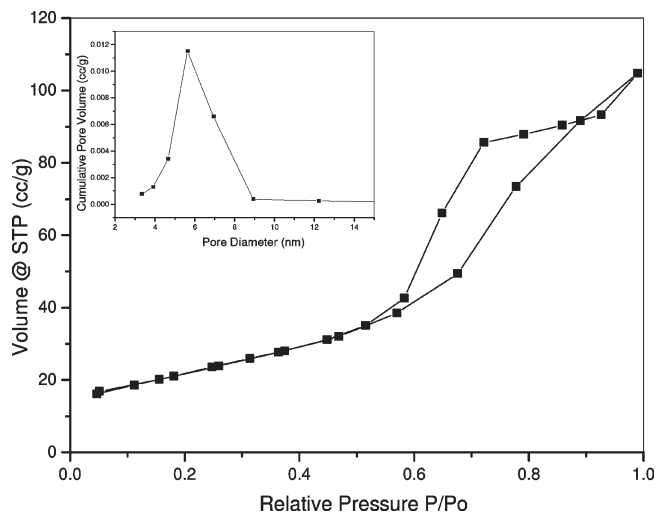


Figure 10. N₂ adsorption–desorption isotherm and the pore size distribution (inset) of 1.5 ED-TiO₂ 400.

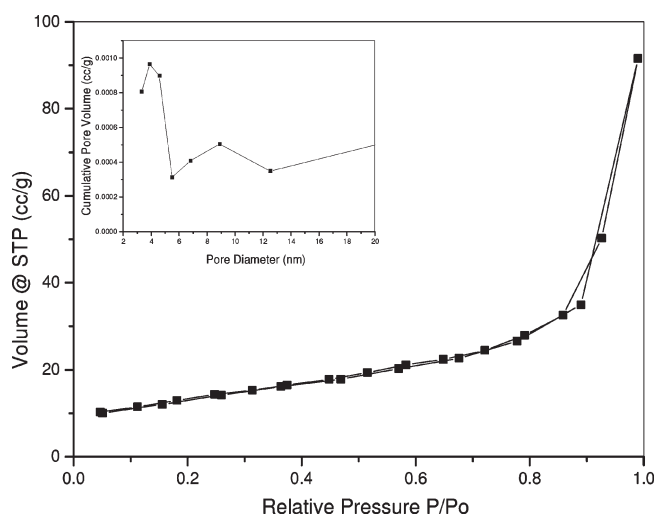


Figure 11. N₂ adsorption–desorption isotherm and the pore size distribution (inset) of Degussa P-25.

Table 2. Textural Properties of Heterojunctions Calcined at Different Temperatures

composition	surface area (m ² /g)	pore diameter (nm)	pore volume (cc/g)
control 400	134.2	4.65	0.209
control 600	40.06	8.16	0.104
1.5 ED-TiO ₂ 400	79.6	5.64	0.168
1.5 ED-TiO ₂ 600	21.28	8.01	0.052
Degussa P-25	46.7	3.89	0.129

543 An increase in pore diameter was also observed with an
544 increase in calcination temperature, which confirms the
545 presence of interstitial pores and its grain growth.⁴⁷
546 Among the samples calcined at 400 °C, the most active
547 catalyst (1.5 ED-TiO₂) showed a larger pore diameter
548 (5.6 nm) than the control sample (4.6 nm) because of the
549 large grain size resulting from the thermally less stable
550 titania precursor. The same composition has a smaller pore
551 size at 600 °C compared to the control sample. This can be
552 due to the densification of powder resulting from excessive
553 grain growth. Even though the heterojunctions have poor

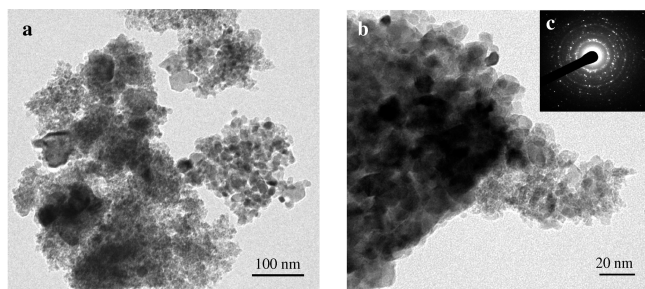


Figure 12. Transmission electron micrograph of 1.5 ED-TiO₂ 400. (a) TEM, (b) HRTEM, and (c) SAED pattern.

554 textural properties in comparison to that of the control sample, properties of the most active heterojunction
555 (1.5 ED-TiO₂ 400) were superior to that of Degussa P-25.
556 Better textural properties of the control sample arise
557 because of the formation of thermally stable acetic acid-
558 Ti⁴⁺ complex,²⁸ and lower textural properties of hetero-
559 junctions result from poor thermal stability of ionic
560 intermediate formed by the reaction between Ti⁴⁺ and
561 EDTA.
562

563 **3.2.7. Transmission Electron Microscopic Studies**
564 **(TEM).** The nanocrystalline structure and phase compo-
565 sition of the most active heterojunction (1.5 ED-TiO₂
566 400) had been investigated by combined high resolution
567 transmission electron microscopy (HRTEM)-selected
568 area electron diffraction (SAED) analysis as shown in
569 Figure 12. The sample was found to be consisting of nano-
570 particles having two different sizes. The average particle
571 size of about 90% of the particles was 10 ± 3 nm, and
572 the remaining 10% were about 15 ± 3 nm in size. These
573 results were consistent with the average crystallite size
574 and anatase-rutile ratio obtained from the XRD analysis
575 (90% 13 nm sized anatase and 10% 18 nm rutile). The
576 15 nm sized rutile nanoparticles were found to be dis-
577 tributed between anatase nanoparticles and thereby faci-
578 litate the formation of heterojunctions (Figure 12 a, b).
579 The selected area electron diffraction (SAED) pattern
580 contains a series of Debye-Scherrer rings that corre-
581 spond to an anatase-rutile mixture (Figure 12 c). The
582 *d*-spacing values 3.38, 2.23, 1.70, and 1.22 Å calculated
583 from the pattern represent the anatase lattice planes with
584 Miller indices (1 0 1), (0 0 4), (1 0 5), and (2 0 4), re-
585 spectively.^{49,50} The rutile lattice planes (1 1 0), (1 0 1),
586 (1 1 1), and (2 2 0) were also identified from the corres-
587 ponding *d*-spacing values of 2.90, 2.5, 2.1, and 1.59 Å.^{49,50} The
588 complex SAED ring pattern confirmed the presence of
589 polycrystalline anatase and rutile nanoparticles oriented
590 in a random manner.⁵⁰

591 **3.3. Photocatalytic Studies.** **3.3.1. Visible Light Photo-**
592 **catalytic Degradation of MB over TiO₂ Heterojunctions.**
593 All N-doped heterojunctions were more visible light
594 active than the control sample or EDTA modified sam-
595 ples with a single phase toward the photocatalytic degra-
596 dation of methylene blue. The most active heterojunction

1.5 ED-TiO₂ 400 containing 90% of 13 nm anatase and
10% of 18 nm rutile shows over 9 times more visible light
activity compared to Degussa P-25 (Figure 13 a, b). Rate
constants obtained for the most active catalyst and
Degussa P-25 were 0.038 and 0.004 min⁻¹, respectively
(Figure 14). Significantly higher visible light activity of
nitrogen doped anatase rutile heterojunctions can be
explained on the basis of band gap narrowing and effi-
cient charge separation at the anatase-rutile interface.
Results obtained from XRD, FT-IR, XPS, and UV/
vis spectroscopy confirmed the formation of N-doped
anatase-rutile heterojunctions having low band gap values.
Additional energy levels created as a result of efficient
doping can utilize visible light for the generation of
electron hole pairs. Asahi et al. explained the visible light
sensitization of N-doped TiO₂ on the basis of Ti-N
bonding. Irie et al. also prepared N-doped TiO₂ by a
NH₃-treatment method.³⁸ They observed the N 1s peak
at 396 and 400 eV in the XPS analysis and ascribed the
396 eV state to visible light sensitization. However, the
results of Diwald et al. rather indicated a negative con-
tribution of Ti-N bonding to photocatalytic activity.⁵¹
So, the contribution of Ti-N bonding to the visible-light
sensitization of TiO₂ has not been completely under-
stood. In our experiments, all nitrogen doped anatase
rutile mixtures at 700 °C with lower nitrogen content
(containing N-Ti-N bonds) show better (except 1:0.5
ED-TiO₂) photocatalytic activity compared to samples at
600 °C (containing O-Ti-N bonds) (Supporting Infor-
mation 12). This behavior can be correlated to the
formation of higher amounts of photocatalytic enhancing
Ti-N bonds at a higher temperature. The discrepancy
observed in the case of 1:0.5 EDTA composition may be
due to the presence of higher amounts of rutile at 700 °C.

In spite of its better textural properties, the control
sample was found to have very low visible light activity
compared to the most active sample, which has poor text-
ural properties but high visible light activity. It is there-
fore evident from the photocatalytic studies that the
textural properties of catalysts are not the only factor
determining the reaction kinetics. It can be concluded
that the composition of heterojunctions and band gap
values contribute more toward the photocatalytic activity
in comparison to the textural properties.

Crystallite sizes of anatase and rutile phases were
smaller for the most active heterojunction (1.5 ED-TiO₂
400) than that in Degussa P-25 (Supporting Information
14). This facilitates the formation of more heterojunc-
tions and thereby increases the activity. It is known that
the conduction band edge of rutile is approximately 0.2
eV lower than that of anatase. On this basis, the model
that the photo excited electrons (from the visible midgap
level) are effectively transferred from the conduction
band of anatase to that of rutile has been proposed
(Figure 16). When a small amount of rutile phase coexists
with anatase phase, the interface between anatase and

(49) Miao, L.; Jin, P.; Kaneko, K.; Terai, A.; Nabatova-Gabain, N.; Tanemura, S. *Appl. Surf. Sci.* **2003**, *212*, 255.

(50) Miao, L.; Tanemura, S.; Kondo, Y.; Iwata, M.; Toh, S.; Kaneko, K. *Appl. Surf. Sci.* **2004**, *238*, 125.

(51) Diwald, O.; Thompson, T. L.; Goralski, E. G.; Walck, S. D.; Yates, J. T. *J. Phys. Chem. B* **2004**, *108*, 52.

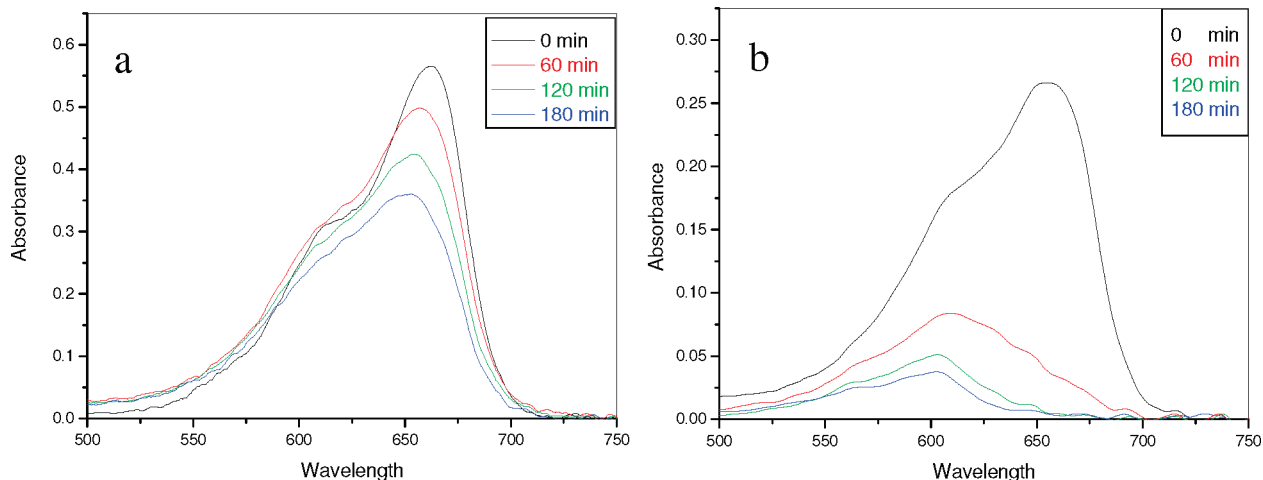


Figure 13. Absorption spectra of visible light induced methylene blue degradation using (a) Degussa P-25 and (b) 1.5 ED-TiO₂ 400.

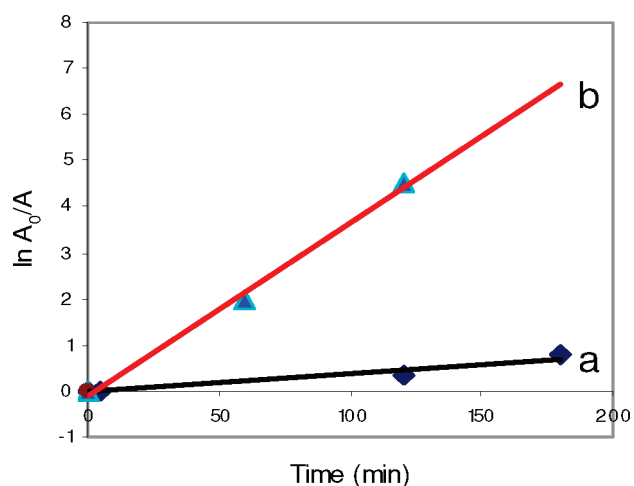


Figure 14. Kinetic study of (a) Degussa P-25 and (b) 1.5 ED-TiO₂ 400.

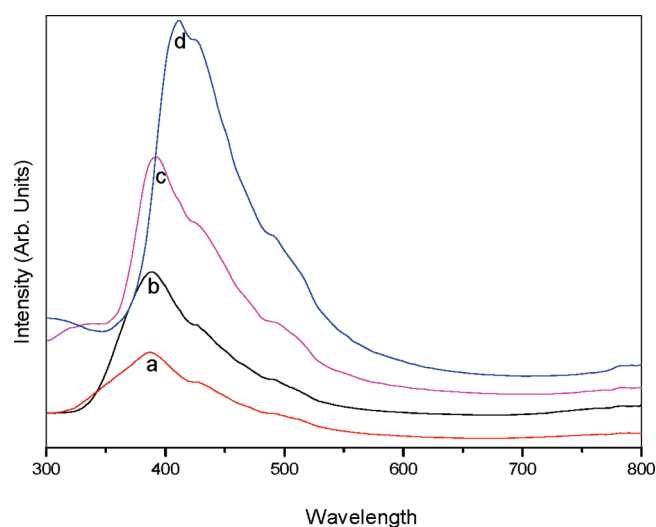


Figure 15. Photo luminescence spectra of samples (a) 1.5 ED-TiO₂ 400, (b) Degussa P-25, (c) pure anatase, and (d) pure rutile.

653 rutile promotes the electron transfer, and rutile works as a
 654 reaction site for photo reduction. Photo oxidation can
 655 take place either on anatase or on the rutile surface. The
 656 heterojunctions obtained at 700 °C containing more Ti–
 657 N bonds showed a higher photocatalytic activity in compar-
 658 ison to those obtained at 600 °C. The most active
 659 heterojunction was the one obtained at 400 °C, and its
 660 highest activity was found to be as a result of optimum
 661 anatase-rutile composition, nanocrystalline nature, and
 662 nitrogen doping. A decrease in photocatalytic activity
 663 was observed for heterojunctions synthesized at higher
 664 temperatures (Supporting Information 12). This can be
 665 due to the formation of a higher amount of rutile phase
 666 having higher electron hole recombination rate, and
 667 decreases in the amount of more photoactive anatase
 668 phase, nitrogen content, and surface area. Higher blue
 669 shift of methylene blue absorption peaks during the
 670 photocatalytic experiment of heterojunction samples in-
 671 dicates faster dye degradation through a N-demethylation
 672 mechanism.^{52,53} The higher visible light photocatalytic

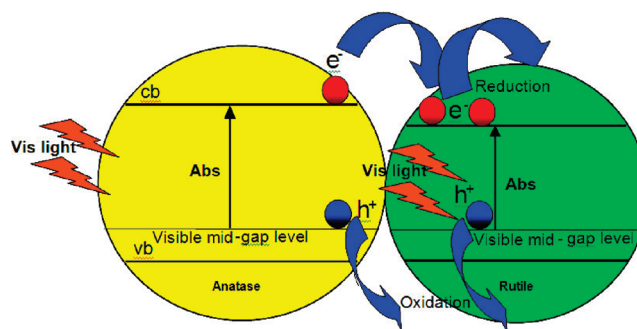


Figure 16. Electron transfer mechanism in N-doped anatase rutile heterojunction.

673 activity observed for the heterojunctions can be therefore,
 674 correlated to the combined band gap narrowing effect of
 675 the nitrogen and electron hole separating effect of rutile.

676 3.3.2. Luminescence Studies. Information regarding
 677 the presence of surface states, formation of photo induced
 678 charge carriers, and their recombination kinetics can be
 679 drawn from the photoluminescence (PL) spectrum of a

(52) Zhang, Y.; Xu, H.; Xu, Y.; Zhang, H.; Wang, Y. *J. Photochem. Photobiol., A* **2005**, *170*, 279.
 (53) Yu, J. R.; Hoi, W. C. *Environ. Sci. Technol.* **2008**, *42*, 294–300.

semiconductor material.⁵⁴ The phenomenon of photocatalysis involves a competitive formation of electron hole pairs and their recombination (radiative or non-radiative). Since defect concentration and life times of photoexcited species play an important role in photocatalysis, investigation of photocatalysts through PL spectroscopy is important to obtain critical reasons behind the enhanced photocatalytic activity. A strong correlation between PL intensity and photocatalytic activity was established by previous research.^{54,55}

Among different samples, pure rutile has highest band-band PL intensity followed by pure anatase, Degussa P-25, and 1.5 ED-TiO₂ 400 (Figure 15). Band-band PL intensities mainly depend on the extent of photoinduced charge carrier separation. The lower band gap and higher surface defects of rutile sample accelerate charge carrier recombination, which reflects as the most intense band-band PL peak.⁵⁶ Efficient electron hole separation resulting from a wider band gap and smaller crystallite size makes anatase less luminescent in comparison to rutile. The lower PL intensity of Degussa P-25 (which is a mixture of 70% anatase and 30% rutile) can be explained on the basis of better electron hole separation resulting from the electron transfer from the conduction band of anatase to that of rutile.⁷ The slight red shift of the band-band transition observed for Degussa P-25 may be due to the presence of more rutile. Among the different N-doped heterojunctions, the lowest PL intensity was observed for sample 1.5 ED-TiO₂ 400. The optimum phase composition (90% anatase + 10% rutile) and nanocrystalline nature of components (which facilitates the formation of more heterojunctions) helps the effective transfer of photo excited electrons from anatase to rutile and slows down the recombination process. Also photoexcited electrons formed on rutile can be transferred to the defect states of anatase, promoting effective charge carrier separation. These processes are responsible for the lower PL intensity and very high photo activity of EDTA modified sample (1.5 ED-TiO₂ 400). Excitonic intensities also follow the same order of band-band intensities because of the same reasons. No additional PL bands from nitrogen impurities were observed for heterojunctions, which eliminated the presence of surface adsorbed nitrogen impurities.

Lower band-band and excitonic PL intensities resulting from efficient charge separation were reported for TiO₂ and ZnO doped with Sn, W, Ag, and Au.^{55,57-61} These semiconductors showing lower PL intensities were also reported to exhibit higher photocatalytic activity.^{59,62} In short, any electron capturing agents can lower both the

band-band and the excitonic PL intensities, which results in an increase in photocatalytic activity. Thus, the lowest PL intensity and the very high visible light activity of nitrogen doped anatase rutile heterojunctions can be explained on the basis of efficient charge separation at the anatase-rutile interface. It is known that the conduction band edge of rutile is approximately 0.2 eV lower than that of anatase.^{7,18} On this basis, the model that the photoexcited electrons (from the visible midgap level) are effectively transferred from the conduction band of anatase to that of rutile has been proposed.

4. Conclusions

Nitrogen doped anatase-rutile heterojunctions having high visible light photocatalytic activity were developed through an ionic intermediate [Ti (H₂O) (edta)]. Low temperature crystallizations of heterojunctions were characterized using DSC, TGA, XRD, HRTEM, and Raman techniques. The nature of dopants was investigated using FT-IR spectroscopy, XRD, and XPS techniques. Conclusive evidence for the formations of both O-Ti-N and N-Ti-N bonds were observed from FT-IR and XPS studies, and substitutional nitrogen doping was found to have an enhancing effect on the photocatalytic activities of heterojunctions. The most active N-doped heterojunction obtained at 400 °C showed a 9-fold enhancement for the visible light decomposition of methylene blue in comparison to the commercial catalyst Degussa P-25. The heterojunction has lower luminescence intensity as a result of better electron hole separation, and better textural properties in comparison to Degussa P-25. The highest photocatalytic activity of the optimum sample (1.5 ED-TiO₂ 400) was due to the combined effect of better electron hole separation, a lower band gap resulting from effective nitrogen doping, and nanocrystalline nature compared to the standard photocatalyst.

Acknowledgment. The authors would like to thank Enterprise Ireland for funding (CFTD/06/IT/326) and Dr. John Colreavy (Director, Centre for Research in Engineering Surface Technology) and Dr. Niall Stobbie for reviewing the paper. The authors would like to dedicate this paper to Professor John M. Kelly, on the occasion of completing his 37 years of teaching and research (celebration of chemistry) at Trinity College Dublin, Ireland.

Supporting Information Available: Further details are given in the supporting tables 1-3 and figures 1-13. This material is available free of charge via the Internet at <http://pubs.acs.org>.

- (54) Liqiang, J.; Yichun, Q.; Baiqi, W.; Shudan, L.; Baojiang, J.; Libin, Y.; Wei, F.; Honggang, F.; Jiazhong, S. *Sol. Energy Mater. Sol. Cells* **2006**, *90*, 1773-1787.
(55) Georgekutty, R.; Seery, M. K.; Pillai, S. C. *J. Phys. Chem. C* **2008**, *112*, 13563-13570.
(56) Gandhe, A. R.; Fernandes, J. B. *J. Solid State Chem.* **2005**, *178*, 2953-2957.
(57) Shang, J.; Yao, W. Q.; Zhu, Y. F.; Wu, N. *Appl. Catal., A* **2004**, *25*, 257.

- (58) Jing, L. Q.; Fu, H. G.; Wang, D. J.; Wei, X.; Sun, J. Z. *Acta Phys. Chim. Sin.* **2005**, *21*, 38.
(59) Li, X. Z.; Li, F. B.; Yang, C. L.; Ge, W. K. *J. Photochem. Photobiol., A* **2001**, *141*, 209.
(60) Xin, B. F.; Jing, L. Q.; Ren, Z. Y.; Wang, B. Q.; Fu, H. G. *J. Phys. Chem. B* **2005**, *109*, 2805.
(61) Li, F. B.; Li, X. Z. *Appl. Catal., A* **2002**, *228*, 15.
(62) Yu, J. G.; Yu, H. G.; Chen, B.; Zhao, X. J.; Yu, J. C.; Ho, W. K. *J. Phys. Chem. B* **2003**, *107*, 13871.